Journal of Alloys and Compounds 509 (2011) 7181–7185

Contents lists available at ScienceDirect

Journal of Alloys and Compounds

journal homepage: www.elsevier.com/locate/jallcom

Enhanced electrochemical performances of multi-walled carbon nanotubes modified $Li_3V_2(PO_4)_3$/C cathode material for lithium-ion batteries

Y.Q. Qiao, J.P. Tu*, Y.J. Mai, L.J. Cheng, X.L. Wang, C.D. Gu

State Key Laboratory of Silicon Materials and Department of Materials Science and Engineering, Zhejiang University, Hangzhou 310027, China

ARTICLE INFO

Article history:
Received 12 February 2011
Received in revised form 23 March 2011
Accepted 7 April 2011
Available online 15 April 2011

Keywords:
Lithium vanadium phosphate
Multi-walled carbon nanotubes
Carbon coating
Lithium-ion battery

ABSTRACT

The multi-walled carbon nanotubes (MWCNTs) modified $Li_3V_2(PO_4)_3$/C composite is synthesized by polyvinyl alcohol (PVA) based carbon-thermal reduction method using MWCNTs as a highly conductive agent. PVA mainly supplies a reductive atmosphere to reduce V^{5+} and provides a network of carbon to inhibit the aggregation of $Li_3V_2(PO_4)_3$ particles. The amorphous carbon coating and MWCNTs co-modified composite shows excellent high-rate lithium intercalation/deintercalation property and cycling performance between 3.0 and 4.3 V. The discharge capacities of 131.7 and 122.9 mAh g^{-1} are obtained at rates of 1 C and 10 C, respectively, for the $Li_3V_2(PO_4)_3$/(C + MWCNTs). These improvements are attributed to the valid conducting networks of C + MWCNTs and the reduced $Li_3V_2(PO_4)_3$ particle size by the network carbon from the pyrolysis of PVA.

1. Introduction

In recent years, lithium ion batteries are considered to have great potential application for electric vehicles (EVs) and hybrid electric vehicles (HEVs) [1–8]. The performance of these batteries depends critically on the properties of their cathode materials. Among cathode materials, monocline $Li_3V_2(PO_4)_3$ is considered to be one of the most promising materials because of its good ion mobility, relatively high operate voltage and large theoretical capacity [9–12]. However, the main disadvantage of $Li_3V_2(PO_4)_3$ is its poor intrinsic conductivity, which presents a major obstacle to practical implementation. Many efforts have been made over the past few years to improve the low conductivity by alien metal doping [13–15] and coating electronically conductive materials [16–20].

It is well known that MWCNTs have many advantages, such as excellent electronic conductivity, small specific surface area and tubular shape [21–24]. It is suggested that the MWCNTs are good additives in the electrode because a more integrated conductive network can be formed between the active materials and the substrate. The batteries with CNT additives in the electrodes presented higher total capacity and better high-rate discharge performance [22,23]. Recently, MWCNTs have introduced as a conductive carbon additive in the preparation of $LiFePO_4$/MWCNTs composites [24,25] and $LiCoO_2$/MWCNTs [26]. Li et al. [24] applied MWCNTs as the conducting additive in $LiFePO_4$ and they found that MWCNTs addition was an effective way to increase rate capability and cycle efficiency. Jin et al. [25] reported that the added MWCNTs in $LiFePO_4$ not only increase the electronic conductivity and lithium-ion diffusion coefficient, but also decrease crystallite size and charge-transfer resistance.

In the present work, polyvinyl alcohol (PVA) based carbon-thermal reduction route by firstly using MWCNTs as a highly conductive agent was adopted to prepare MWCNTs-modified $Li_3V_2(PO_4)_3$/C. Herein, PVA is mainly supplying a reductive atmosphere to reduce V^{5+} and providing a network of carbon to inhibit the aggregation of $Li_3V_2(PO_4)_3$ particles. Foremost, the MWCNTs and the network carbon from the pyrolysis of PVA will link the $Li_3V_2(PO_4)_3$ particles effectively, which expect the MWCNTs-modified $Li_3V_2(PO_4)_3$/C composite to achieve a high-rate lithium intercalation/deintercalation property.

2. Experimental

MWCNTs-modified $Li_3V_2(PO_4)_3$/C composite was prepared by carbon-thermal reduction method, both PVA and MWCNTs were used as carbon source in this study (denoted as $Li_3V_2(PO_4)_3$/(C + MWCNTs)). The details about the synthesis of MWCNTs were introduced elsewhere [27]. Stoichiometric of Li_2CO_3, NH_4VO_3, $NH_4H_2PO_4$ and appropriate amount of PVA + MWCNTs (PVA:MWCNTs = 1:1, wt.%) were mixed in ethanol and ball milled for 4 h. After ethanol was evaporated, the precursor was heated at 850 °C for 10 h in argon flowing. For comparison, $Li_3V_2(PO_4)_3$/C composite without MWCNTs was also prepared using the same process. The amounts of residual carbon in the $Li_3V_2(PO_4)_3$/(C + MWCNTs) and $Li_3V_2(PO_4)_3$/C were 4.71 and 5.27 wt.%, respectively, measured by elemental analyzer (EA, Flash EA1112). Electrical conductivity measurements were carried on CON510, the powders were hot-pressed respectively in a graphite die for 1 h with T = 500 °C, P = 80 MPa in a vacuum uni-axial compressor. The structure and morphology of the as-prepared powders were characterized using X-ray diffraction (XRD, Philips PC-APD with Cu K radiation) and

* Corresponding author. Tel.: +86 571 87952856; fax: +86 571 87952573.
E-mail addresses: tujp@zju.edu.cn, tujp@zjuem.zju.edu.cn (J.P. Tu).

0925-8388/$ – see front matter © 2011 Elsevier B.V. All rights reserved.
doi:10.1016/j.jallcom.2011.04.048

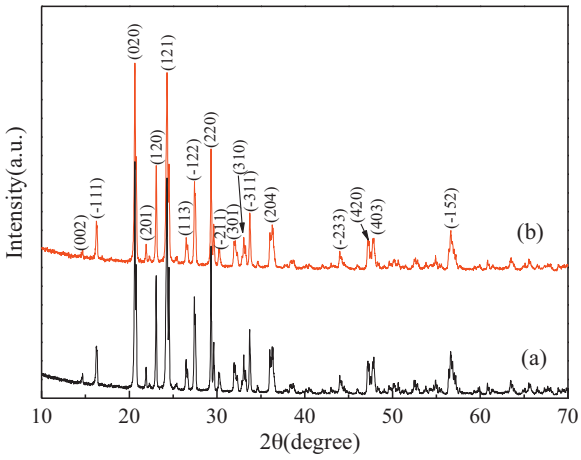

Fig. 1. XRD patterns of (a) $Li_3V_2(PO_4)_3$/(C + MWCNTs) and (b) $Li_3V_2(PO_4)_3$/C.

high-resolution transmission electron microscopy (TEM, Tecnai G2 F30 S-Twin).

Electrochemical performances of the composites were characterized using CR2025 coin-type cell. A metallic lithium foil served as the anode electrode. The cathode consisted of 85 wt.% active material, 10 wt.% carbon conductivity (residual carbon and acetylene black) and 5 wt.% polyvinylidene fluoride (PVDF) on aluminum foil. 1 M $LiPF_6$ in ethylene carbonate (EC)-dimethyl carbonate (DMC) (1:1 in volume) as the electrolyte, and a polypropylene micro-porous film (Cellgard 2300) as the separator. The cells were assembled in a glove box filled with high-purity argon. The charge–discharge tests were carried out on LAND battery test system (Wuhan, China) between 3.0 and 4.3 V by applying from 0.5 C to 10 C. Cyclic voltammetry (CV) test was carried out using the CHI660 C electrochemical workstation in a potential range of 3.0–4.3 V (vs. Li/Li^+) at a scan rate of 0.1 mV s^{-1}. For electrochemical impedance spectroscopy (EIS) measurements, the test cells were with the metallic lithium foil as both the reference and counter electrodes. EIS measurements were performed on the CHI660 C over a frequency range of 100 kHz to 10 mHz at a stage of charge (3.6 V vs. Li/Li^+) by applying an AC signal of 5 mV.

3. Results and discussion

Fig. 1 shows the XRD patterns of $Li_3V_2(PO_4)_3$/(C + MWCNTs) and $Li_3V_2(PO_4)_3$/C composites. All the peaks can be assigned to monoclinic $Li_3V_2(PO_4)_3$ (space group $P2_1/n(14)$, ICSD #96962) and no impurities can be observed. Additionally, the added MWCNTs and

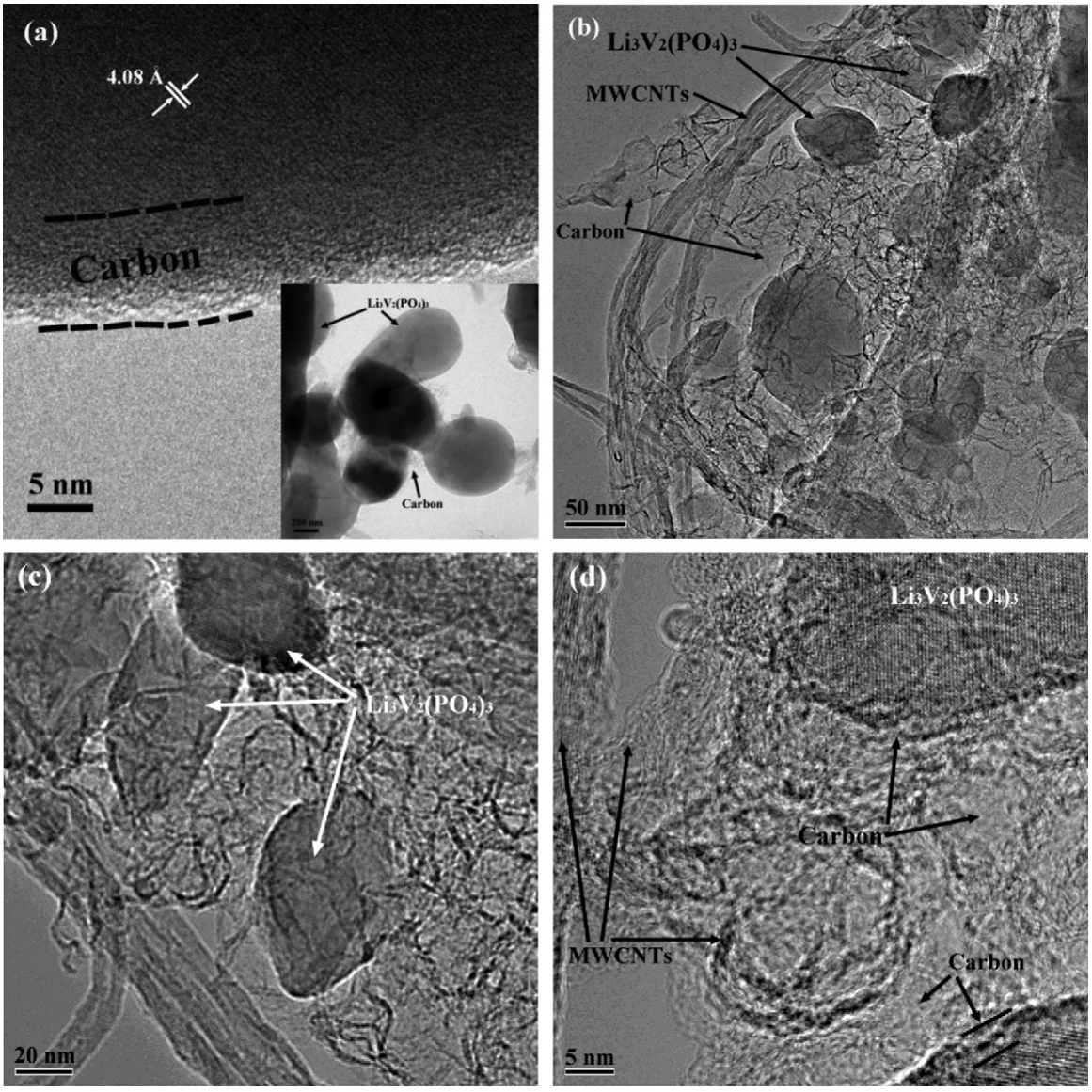

Fig. 2. TEM images of (a) $Li_3V_2(PO_4)_3$/C and (b) $Li_3V_2(PO_4)_3$/(C + MWCNTs); (c) and (d) enlarged TEM images showing valid conducting network by carbon and MWCNTs.

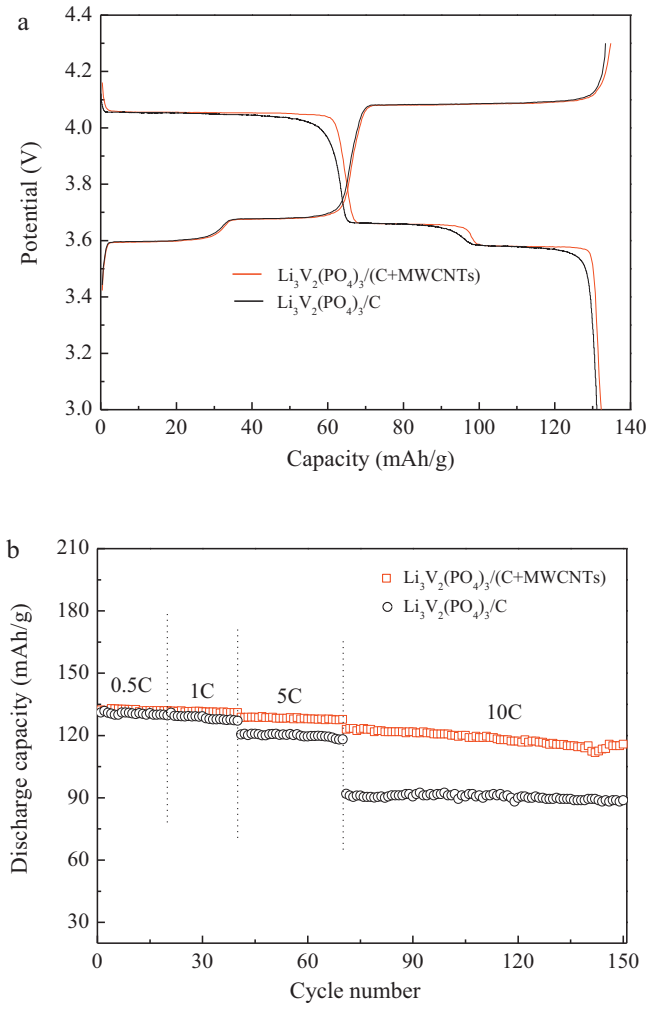

Fig. 3. (a) The charge–discharge curves for $Li_3V_2(PO_4)_3$/(C + MWCNTs) and $Li_3V_2(PO_4)_3$/C electrodes between 3.0 and 4.3 V at 0.5 C; (b) Rate performance of $Li_3V_2(PO_4)_3$/(C + MWCNTs) and $Li_3V_2(PO_4)_3$/C at different charge–discharge rates between 3.0 and 4.3 V.

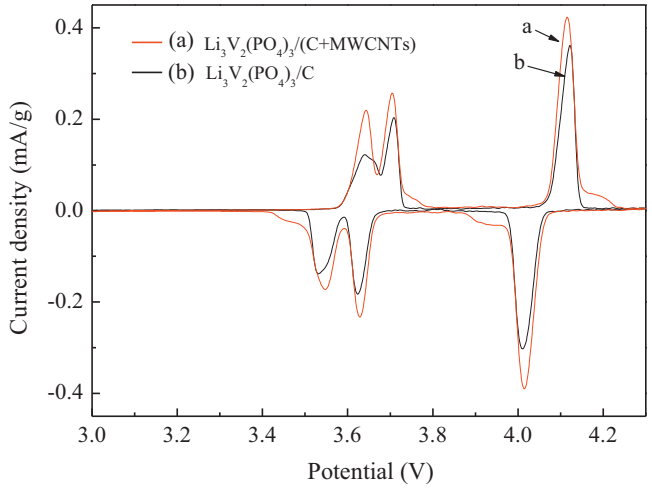

Fig. 4. CV curves of (a) $Li_3V_2(PO_4)_3$/(C + MWCNTs) and (b) $Li_3V_2(PO_4)_3$/C in a potential range of 3.0–4.3 V at a scan rate of 0.1 mV s^{-1}.

PVA do not change the crystal structure of $Li_3V_2(PO_4)_3$ which is similar to those in previous reports [3,9,19]. Otherwise, no additional diffraction peak related-carbon is detected in the XRD patterns, which is attributed to the amorphous state of the residual carbon, or the amount of carbon is too low to be detected.

Fig. 2a shows the TEM image of $Li_3V_2(PO_4)_3$/C. It can be observed that the $Li_3V_2(PO_4)_3$ particles are coated with a uniform carbon layer about 8 nm in thickness. The 4.08 Å spacing corresponds to the (0 1 2) plane of monoclinic $Li_3V_2(PO_4)_3$. Dissociative amorphous carbon can also be found between the particles. It is well known that the residual carbon from pyrolysis of organics or polymers is able to inhibit the aggregation of $Li_3V_2(PO_4)_3$ particles and provide good contact between the particles [16–18]. Electronic conductivity measurement illustrates that the electrical conductivity of the as-prepared $Li_3V_2(PO_4)_3$/C composite is 4.95×10^{-3} S cm^{-1}, which is much higher than that of the uncoated $Li_3V_2(PO_4)_3$ (2.3×10^{-7} S cm^{-1}) [28]. In order to distinguish between the MWCNTs and $Li_3V_2(PO_4)_3$/C, TEM analysis were also conducted. As illustrated in Fig. 2b and c, the $Li_3V_2(PO_4)_3$/C particles are well modified by MWCNTs with the help of the PVA. On the assumption that PVA was not used in Figs. 2b and c, only two or even three particles could be connected by MWCNTs. However, when the combination of PVA and MWCNTs was employed during the process, the network carbon from the pyrolysis of PVA is able to link the MWCNTs to the $Li_3V_2(PO_4)_3$ particles effectively, making more particles interlink with each other. On the other hand, the electrical conductivity of the as-prepared $Li_3V_2(PO_4)_3$/(C + MWCNTs) composite is increased to 1.13 S cm^{-1} when MWCNTs was added to the mixture, which is two orders of magnitude higher than that of $Li_3V_2(PO_4)_3$/C. Fig. 2d shows an enlarged TEM image of the $Li_3V_2(PO_4)_3$/(C + MWCNTs) composite. It is clearly that the $Li_3V_2(PO_4)_3$ particles are coated with carbon, and the dissociative amorphous carbon can link the MWCNTs to the $Li_3V_2(PO_4)_3$ particles effectively, forming a valid conducting network. Therefore, it can be speculated that this valid conducting networks will result in excellent electrochemical performance of $Li_3V_2(PO_4)_3$/(C + MWCNTs) composite.

Fig. 3 shows the charge–discharge curves of $Li_3V_2(PO_4)_3$/(C + MWCNTs) and $Li_3V_2(PO_4)_3$/C electrodes in the potential range of 3.0–4.3 V at 0.5 C rate. Both the cells exhibit three charge plateaus and correspondingly three discharge plateaus, which are identified as the two-phase transition processes during the electrochemical reactions [6,7]. Compared to the $Li_3V_2(PO_4)_3$/C, the $Li_3V_2(PO_4)_3$/(C + MWCNTs) electrode has longer charge/discharge curves and smaller potential differences of the plateaus, which manifests that the MWCNTs-modified $Li_3V_2(PO_4)_3$/C composite has lower electrochemical polarization and leads to better reversibility in the charge–discharge processes. In the potential range of 3.0–4.3 V, two Li-ions in the $Li_3V_2(PO_4)_3$ can be removed, and its theoretical capacity is 133 mAh g^{-1} between 3.0 and 4.3 V. It can be found that the $Li_3V_2(PO_4)_3$/(C + MWCNTs) electrode exhibits a high initial discharge capacity of 132.3 mAh g^{-1} (very close to its theoretical capacity), which is higher than that of $Li_3V_2(PO_4)_3$/C (131.1 mAh g^{-1}). What is more, the effect of the C + MWCNTs is even more significant from the rate performance at different current densities, as shown in Fig. 3b. The discharge capacities of 131.7 and 122.9 mAh g^{-1} are obtained at rates of 1 C and 10 C, respectively, for the $Li_3V_2(PO_4)_3$/(C + MWCNTs), whereas the values drop from 131.0 mAh g^{-1} (1 C) to 91.9 mAh g^{-1} (10 C) for the $Li_3V_2(PO_4)_3$/C. It is also observed that about 92.9% of its capacity remains on going from 0.5 C to 10 C rate, for the $Li_3V_2(PO_4)_3$/(C + MWCNTs) electrode, such an improved kinetics can be attributed to the fast charge transport between the electrolyte and the particles on account of the valid conducting networks of C + MWCNTs [23,24]. It has been reported that the carbon coating can retard formation of the SEI film in the surface of

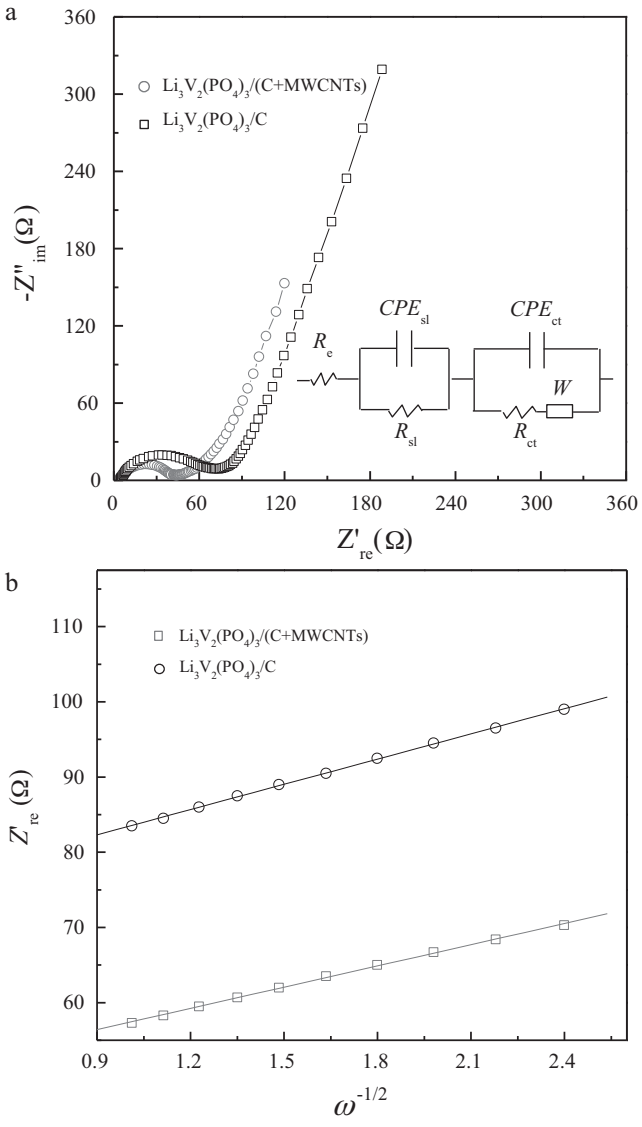

Fig. 5. (a) Nyquist plots of $Li_3V_2(PO_4)_3$/(C + MWCNTs) and $Li_3V_2(PO_4)_3$/C measured at the charge potential of 3.6 V (vs. Li/Li^+). (b) The relationship plot between Z_{re} and $\omega^{-1/2}$ at low-frequency region.

the particles and also decrease the charge-transfer impedance [16]. The C + MWCNTs can provide a good network for low-conductance $Li_3V_2(PO_4)_3$, thus the electronic conductivity was improved significantly due to the valid conducting networks in $Li_3V_2(PO_4)_3$, making an enhanced rate capability of $Li_3V_2(PO_4)_3$/(C + MWCNTs).

Fig. 4 shows the CV curves of $Li_3V_2(PO_4)_3$/(C + MWCNTs) and $Li_3V_2(PO_4)_3$/C. Noticeably, the anodic/cathodic peaks of MWCNTs modified $Li_3V_2(PO_4)_3$/C are more symmetrical and sharper than that of $Li_3V_2(PO_4)_3$/C composite, which indicates the better electrochemical reversibility. Furthermore, the potential separations of $Li_3V_2(PO_4)_3$/(C + MWCNTs) between the anodic and cathodic peaks are less than that of $Li_3V_2(PO_4)_3$/C, which also demonstrates the reversibility and reactivity of $Li_3V_2(PO_4)_3$/(C + MWCNTs) are enhanced due to the presence of valid conducting networks of C + MWCNTs.

Fig. 5a shows the Nyquist plots of $Li_3V_2(PO_4)_3$/(C + MWCNTs) and $Li_3V_2(PO_4)_3$/C measured at the charge potential of 3.6 V after 5 cycles. In order to clearly illuminate the AC impedance spectra of the electrodes, an equivalent circuit has been built in Fig. 5a. R_e represents the solution resistance of the electrolyte; R_{sl} and CPE_{sl} designate the migration resistance of lithium ions and the capacity of surface layer, respectively; R_{ct} and CPE_{ct} stand for the charge-transfer resistance and double-layer capacitance, respectively; W represents the diffusion-controlled Warburg impedance [24,29–31]. It is found that the R_e is similar for the two electrodes, and the R_e values of $Li_3V_2(PO_4)_3$/(C + MWCNTs) and $Li_3V_2(PO_4)_3$/C are 4.52 Ω and 4.73 Ω, respectively, which are much lower than those of R_{sl} and R_{ct}. The migration resistance of lithium ions R_{sl} of $Li_3V_2(PO_4)_3$/(C + MWCNTs) and $Li_3V_2(PO_4)_3$/C is 12.31 Ω and 19.38 Ω, respectively. The simulated charge-transfer resistance R_{ct} of $Li_3V_2(PO_4)_3$/(C + MWCNTs) and $Li_3V_2(PO_4)_3$/C is 22.36 Ω and 41.12 Ω, respectively. It can be found that the $Li_3V_2(PO_4)_3$/(C + MWCNTs) electrode exhibits a smaller charge-transfer resistance, which indicates the formation of conductive network by C + MWCNTs can increase the conductivity of active materials and reduce the impedance remarkably.

The diffusion coefficient of Li^+ can be derived from the following Eq. (1) [32,33] or Eq. (2) [25,32].

$$D_{Li} = \frac{1}{2}\left(\frac{V_m}{FA\sigma_w}\right)^2\left(\frac{dE}{dx}\right)^2 \quad (1)$$

$$D_{Li} = \frac{R^2T^2}{2A^2n^4F^4\sigma_w^2C^2} \quad (2)$$

where V_m is the molar volume, F is Faraday constant, A is the active surface area, σ_w is the Warburg factor, dE/dx is the slope of the open-circuit voltage vs. mobile Li^+ concentration x, D_{Li} is the apparent diffusion coefficient, R is the gas constant, T is the absolute temperature, n is the number of electrons per molecule during oxidization, and C is the molar concentration of Li^+. At the charge state of 3.6 V, the electrochemical reaction is in the two-phase region. It can easily find that the value of dE/dx is almost zero [32,33], thus without any meaning for Eq. (1). Therefore, we select Eq. (2) to calculate the apparent D_{Li} values.

The σ_w was determined as the value of the slope of Z_{re} vs. $\omega^{-1/2}$ for the Warburg region [25,32]. The relationship plots between Z_{re} and $\omega^{-1/2}$ at low-frequency region are shown in Fig. 5b. Thus, based on Eq. (2), the apparent diffusion coefficient of Li-ions for $Li_3V_2(PO_4)_3$/(C + MWCNTs) and $Li_3V_2(PO_4)_3$/C is 6.2×10^{-9} and 2.4×10^{-9}, respectively. It is noticed that the diffusion coefficient of $Li_3V_2(PO_4)_3$/(C + MWCNTs) is enhanced by MWCNTs adding, which can be attributed to its higher electronic conductivity [18,31,34].

4. Conclusions

MWCNTs-modified $Li_3V_2(PO_4)_3$/C composite was successfully synthesized by PVA based carbon-thermal reduction method. Compared with the $Li_3V_2(PO_4)_3$/C and $Li_3V_2(PO_4)_3$/MWCNTs composites, the formation of conductive network by C + MWCNTs on $Li_3V_2(PO_4)_3$ particles has been greatly improved by using of PVA. This co-modified material exhibited improved cycling performance and good high-rate lithium intercalation/deintercalation properties. At a charge–discharge rate of 10 C, it can deliver a capacity of 122.9 mAh g^{-1}, much higher than that of $Li_3V_2(PO_4)_3$/C.

References

[1] X.-L. Wu, L.-Y. Jiang, F.-F. Cao, Y.-G. Guo, L.-J. Wan, Adv. Mater. 21 (2009) 2710.
[2] M. Yang, Q.M. Gao, J. Alloys Compd. 509 (2011) 3690.
[3] H. Huang, T. Faulkner, J. Barker, M.Y. Saidi, J. Power Sources 189 (2009) 748.
[4] C.G. Son, H.M. Yang, G.W. Lee, A.R. Cho, V. Aravindan, H.S. Kim, W.S. Kim, Y.S. Lee, J. Alloys Compd. 509 (2011) 1279.
[5] J. Zhong, X.L. Wang, X.H. Xia, C.D. Gu, J.Y. Xiang, Y. Zhou, J. Zhang, J.P. Tu, J. Alloys Compd. 509 (2011) 3889.
[6] M.X. Gao, Y. Lin, Y.H. Yin, Y.F. Liu, H.G. Pan, Electrochim. Acta 55 (2010) 8043.
[7] X.Y. Wang, S.Y. Yin, K.L. Zhang, Y.X. Zhang, J. Alloys Compd. 486 (2009) L5.
[8] X.H. Huang, J.P. Tu, B. Zhang, C.Q. Zhang, Y. Li, Y.F. Yuan, H.M. Wu, J. Power Sources 161 (2006) 541.

[9] H. Huang, S.-C. Yin, T. Kerr, N. Taylor, L.F. Nazar, Adv. Mater. 14 (2002) 1525.
[10] B. Huang, X.P. Fan, X.D. Zheng, M. Lu, J. Alloys Compd. 509 (2011) 4765.
[11] E. Kobayashi, L.S. Plashnitsa, T. Doi, S. Okada, J.-I. Yamaki, Electrochem. Commun. 12 (2010) 894.
[12] J. Zhai, M.S. Zhao, D.D. Wang, Y.Q. Qiao, J. Alloys Compd. 502 (2010) 401.
[13] J.S. Huang, L. Yang, K.Y. Liu, Y.F. Tang, J. Power Sources 195 (2010) 5013.
[14] S.-Q. Liu, S.-C. Li, K.-L. Huang, B.-L. Gong, G. Zhang, J. Alloys Compd. 450 (2008) 499.
[15] Q. Kuang, Y.M. Zhao, X.N. An, J.M. Liu, Y.Z. Dong, L. Chen, Electrochim. Acta 55 (2010) 1575.
[16] Y.Z. Li, Z. Zhou, X.P. Gao, J. Yan, Electrochim. Acta 52 (2007) 4922.
[17] Y.Q. Qiao, X.L. Wang, Y. Zhou, J.Y. Xiang, D. Zhang, S.J. Shi, J.P. Tu, Electrochim. Acta 56 (2010) 510.
[18] T. Jiang, Y.J. Wei, W.C. Pan, Z. Li, X. Ming, G. Chen, C.Z. Wang, J. Alloys Compd. 488 (2009) L26.
[19] L. Zhang, J.P. Tu, J.Y. Xiang, Y. Zhou, X.L. Wang, S.J. Shi, J. Power Sources 195 (2010) 5057.
[20] Y.Q. Qiao, X.L. Wang, J.Y. Xiang, D. Zhang, W.L. Liu, J.P. Tu, Electrochim. Acta 56 (2011) 2269.
[21] D.J. Yang, S.G. Wang, Q. Zhang, P.J. Sellin, G. Chen, Phys. Lett. A 329 (2004) 207.
[22] J.B. Wu, J.P. Tu, Z. Yu, X.B. Zhang, J. Electrochem. Soc. 153 (2006) A1847.
[23] J.Y. Xiang, J.P. Tu, J. Zhang, J. Zhong, D. Zhang, J.P. Cheng, Electrochem. Commun. 12 (2010) 1103.
[24] X.L. Li, F.Y. Kang, X.D. Bai, W.C. Shen, Electrochem. Commun. 9 (2007) 663.
[25] B. Jin, E.M. Jin, K.-H. Park, H.-B. Gu, Electrochem. Commun. 10 (2008) 1537.
[26] Q.-T. Zhang, M.-Z. Qu, H. Niu, Z.-L. Yu, New Carbon Mater. 22 (2007) 361.
[27] J.P. Cheng, X.B. Zhang, Y. Ye, J. Solid State Chem. 179 (2006) 91.
[28] S.-C. Yin, P.S. Strobel, H. Grondey, L.F. Nazar, Chem. Mater. 16 (2004) 1456.
[29] X.K. Zhi, G.C. Liang, L. Wang, X.Q. Ou, L.M. Gao, X.F. Jie, J. Alloys Compd. 503 (2010) 370.
[30] T. Jiang, C.Z. Wang, G. Chen, H. Chen, Y.J. Wei, X. Li, Solid State Ionics 180 (2009) 708.
[31] T. Jiang, F. Du, K.J. Zhang, Y.J. Wei, Z. Li, C.D. Wang, G. Chen, Solid State Sci. 12 (2010) 1672.
[32] T. Jiang, W.C. Pan, J. Wang, X.F. Bie, F. Du, Y.J. Wei, C.Z. Wang, G. Chen, Electrochim. Acta 55 (2010) 3864.
[33] X.H. Rui, J. Liu, C. Li, C.H. Chen, Electrochim. Acta 55 (2010) 2384.
[34] L.A. Montoro, J.M. Rosolen, Electrochim. Acta 49 (2004) 3243.